Smart molecular/MoS_2 heterostructures featuring light and thermally-induced strain driven by spin switching

Ramón Torres-Cavanillas, Marc Morant-Giner, Garin Escorcia-Ariza, Julien Dugay, Josep Canet-Ferrer, Sergio Tatay, Salvador Cardona-Serra, Mónica Giménez-Marqués, Marta Galbiati, Alicia Forment-Aliaga and Eugenio Coronado**

Instituto de Ciencia Molecular (ICMol), Universidad de Valencia, C/ Catedrático José Beltrán 2, Paterna, 46980, Spain.
E-mail: alicia.forment@uv.es and eugenio.coronado@uv.es

Keywords: spin-crossover, transition metal dichalcogenides, nanoparticles, strain, 2D heterostructure, molybdenum disulfide

In this work we exploit the ability of spin-crossover molecules to switch between two spin states, upon the application of external stimuli, to prepare smart molecular/2D heterostructures. Through the chemical design of the hybrid interface, that involves a covalent grafting between the two components, we obtain a hybrid heterostructure formed by spin-crossover nanoparticles anchored on chemically functionalized monolayers of semiconducting MoS_2. In the resulting hybrid, the strain generated by the molecular system over the MoS_2 layer, as a consequence of a thermal or light-induced spin switching, results in a dramatic and reversible change of its electrical and optical properties. This novel class of smart molecular/2D heterostructures could open the way towards a novel generation of hybrid multifunctional materials and devices of direct application in highly topical fields like electronics, spintronics or molecular sensing.

The research on graphene and other two-dimensional (2D) materials has been propelled by the possibility of studying and exploiting the properties of matter in the 2D limit.[1] Nowadays, this topic is moving towards the assembly of monolayers of different types to afford van der Waals heterostructures.[2-4] In the 2D area, apart from the chemical functionalization of 2D materials,[5] the use of molecules as precursors, constituents or functional components of novel 2D systems and heterostructures, has been scarcely investigated.[6,7] An interesting possibility in this context deals with the fabrication of mixed molecular/2D heterostructures, in which the properties of the "all surface" 2D layer can be tuned by the hybrid interface, i.e., by the interactions established between the molecules and the 2D material.[8,9]

A versatile family of 2D layered materials in which this molecular/2D concept can be exploited, is that formed by transition metal dichalcogenides (TMDCs)[10-12] of formula MX_2 (M = metals traditionally restricted to groups IV–VII; X = S, Se, Te). The members of this family display a wide range of electronic properties as a function of their composition and structures, including insulating, semiconducting, metallic and superconducting properties. Among them, the most deeply studied system is MoS_2, owing to its chemical stability, and electronic properties. The weak interaction between stacked layers makes it feasible to isolate monolayers of this material, create van der Waals heterostructures and exploit them to design hybrid structures and electronic devices displaying new low-dimensional physics and unique functionalities.[13] Of special interest is the correlation between the electronic structure and the structural arrangement of S atoms in the monolayer. In fact, by a slight gliding of the S atoms, a switching between a trigonal prismatic symmetry around the Mo atom (2H-phase) and an octahedral one (1T-phase) occurs, giving rise to an electronic modulation of the 2D material from semiconducting to metallic.[14] This phase transition from 2H to 1T can be induced by different external stimuli such as chemical modification[15,16] or electron beam radiation,[17] while the inverse process can be achieved by thermal treatment,[18] infrared radiation,[19] or aging of the material.[20] An attractive possibility in this context is to induce the phase transition by applying strain. This has been

theoretically predicted[21,22] and experimentally demonstrated in ultrathin MoS_2 layers in which a band gap narrowing under low tensile strain has been achieved, which enables the reversible tuning of their optical and electronic properties.[23,24] Sophisticated devices have been reported to prove the strain modulation of both the optical and electronic band gaps, through photoluminescence (PL), Raman spectroscopy,[25-27] and transport measurements.[27,28] In addition, an intrinsic negative piezoresistivity has been observed[24] and exploited to develop a piezoresistive composite in which the resistance decreases when the strain increases (negative Gauge factor).[29]

In this scenario, we have envisioned the possibility of preparing MoS_2-based heterostructures where the second component is an active molecular system that can directly and reversibly tune the strain applied on the 2D material and, therefore, its electronic structure and electric conductivity. We have chosen switchable molecular-based spin-crossover (SCO) materials for this purpose. These materials are, in most cases, Fe(II) compounds that undergo spin transition between low spin (LS with S=0) and high spin (HS with S=2) configurations upon the application of an external stimulus such as light, temperature, pressure or chemical activation. This spin transition comes along with an intrinsic change in volume (up to 11.5%)[30] and a variation of their mechanical,[31] magnetic,[32] electrical[33] and optical properties.[34] Interesting devices[35] and composites based on SCO materials embedded in different polymers have been already reported where a change in volume upon spin transition induces strain effects on a second component modifying their electrical and/or mechanical properties.[36-38]

However, in the field of 2D materials, the inducement of strain by phase transition materials has not been demonstrated so far. The first example of SCO/2D heterostructure was based on the deposition of SCO nanoparticles on graphene. In this case, the thermal spin transition of the nanoparticles resulted in significant changes in the transport properties of graphene. However, the origin of these electrical changes was electronic rather than mechanical. In fact, it was ascribed to the interaction of the graphene electrons with the phonons of the SCO

nanoparticles.[39] Just very recently, an inverse approach has been followed, consisting in the deposition of a mechanically-exfoliated graphene layer on a large SCO crystal with a polymeric spacer in between. Nevertheless, in this transistor geometry, the mechanical influence of the SCO crystal over the properties of the 2D layer is attenuated by the presence of the spacer, thus resulting in a small modification of graphene conductivity, mainly attributed to changes in the induced electrostatic potential. [40]

In the present work, we focus on SCO nanoparticles as phase transition material to induce a strain on the 2D material and thus modulate its electrical and optical properties. These nanoparticles are based on the $[Fe(Htrz)_2(trz)](BF_4)$ coordination polymer (Htrz = 1,2,4-triazole and trz = triazolate) covered with a silica shell (from now on SCO-NPs).[41,42] These core/shell nanoparticles have shown to undergo a cooperative spin transition near room temperature and, depending on the purpose, their sizes and composition can be tuned.[43,44] In addition, the silica shell not only preserves the chemical stability of the SCO system, but also provides an anchoring point for their further chemical functionalization, giving rise to robust heterostructures.[41]

Results

Chemical design of a hybrid SCO/MoS_2 heterostructure. In order to prepare the hybrid SCO/MoS_2 heterostructures, a straightforward solution grafting protocol that coats MoS_2 flakes with pre-synthesized SCO-NPs has been developed. This involves the chemical functionalization with 3-iodopropyl(trimethoxysilane) (IPTS) of ultrathin chemically exfoliated MoS_2 layers (CE-MoS_2), followed by the anchoring of the SCO-NPs to these functionalized layers via a covalent bond between the trimethoxysilane group and the silica shell[41,45] (**Fig. 1**). In more detail, this protocol starts with the preparation of CE-MoS_2 layers by reacting bulk 2H-MoS_2 with *n*-butyllithium (*n*-BuLi) used as reducing species.[46] During this process an electron transfer to MoS_2 occurs, giving rise to a partial structural reorientation and

an electronic band structure modification, that triggers the transition from the semiconducting 2H to the metallic 1T-phase,[14,47] as confirmed by X-ray photoelectron (XPS) and Raman spectroscopies (**Fig. 2** and **Table S1**). After re-dispersion, the CE-MoS_2 flakes retain an excess of negative charge on their surfaces (**Fig. S1**),[48] providing high colloidal stability and facilitating their ulterior covalent functionalization. On the other hand, core-shell SCO-NPs are synthesized following the protocol reported by some of us[44] (see Methods).

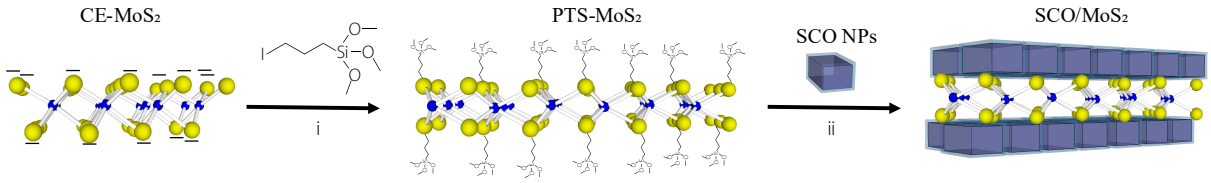

Fig. 1. Schematic representation of the synthetic approach to prepare SCO/MoS_2 hybrid heterostructures. (i) CE-MoS_2 is covalently functionalized with propyl(trimethoxysilane) (PTS) groups by reaction with 3-iodopropyl(trimethoxysilane) (IPTS); (ii) SCO-NPs, which are covered by a thin SiO_2 shell, are covalently attached to the functionalized MoS_2 layers through a chemical reaction between the trimethoxysilane group and the SiO_2 shell.

In order to functionalize the MoS_2 layers, a CE-MoS_2 suspension is mixed with a 3-iodopropyl(trimethoxysilane) (IPTS) solution. The excess of negative charge accumulated in CE-MoS_2 facilitates the nucleophilic attack to IPTS, resulting in the displacement of I and the formation of new covalent S-C bonds.[49] This gives rise to MoS_2 flakes decorated with propyltrimethoxysilane groups (PTS-MoS_2) (**Fig. 1**, step i). The successful anchoring of the IPTS onto the MoS_2 surface is evidenced by a clear decrease in the measured ξ-potential value (from -30 mV to -4 mV, **Fig. S1**).[49] XPS confirms that functionalization takes place without modification of Mo and S oxidation states (**Fig. 2a** and **b**). However, during the process, CE-MoS_2 S2p, and Mo3d peaks blue shift ~1 eV (**Table S1**), suggesting a phase transition from the metallic 1T into the semiconducting 2H-phase. This conversion is confirmed in PTS-MoS_2 Raman spectrum where J peaks at 152, 232 and 326 cm^{-1} (fingerprint of the metallic phase)[50], decrease substantially at the expense of E^1_{2g} and A_{1g} peaks (**Fig. 2c**). Moreover, PL signal is restored, further supporting the conversion to the semiconducting phase[50,51] (**Fig. 2d**). These results contrast with those reported by Chhowalla and coworkers where 1T-phase was preserved

after functionalization but with unusual semiconducting properties and intense photoluminescence recovery.[49] Such a difference may be related with our higher degree of functionalization of the MoS_2 units (~30 % according to thermogravimetric analysis; **Fig. S2**), which could be originated in our higher ratio of 1T-phase in the starting CE-MoS_2 (~85 %).

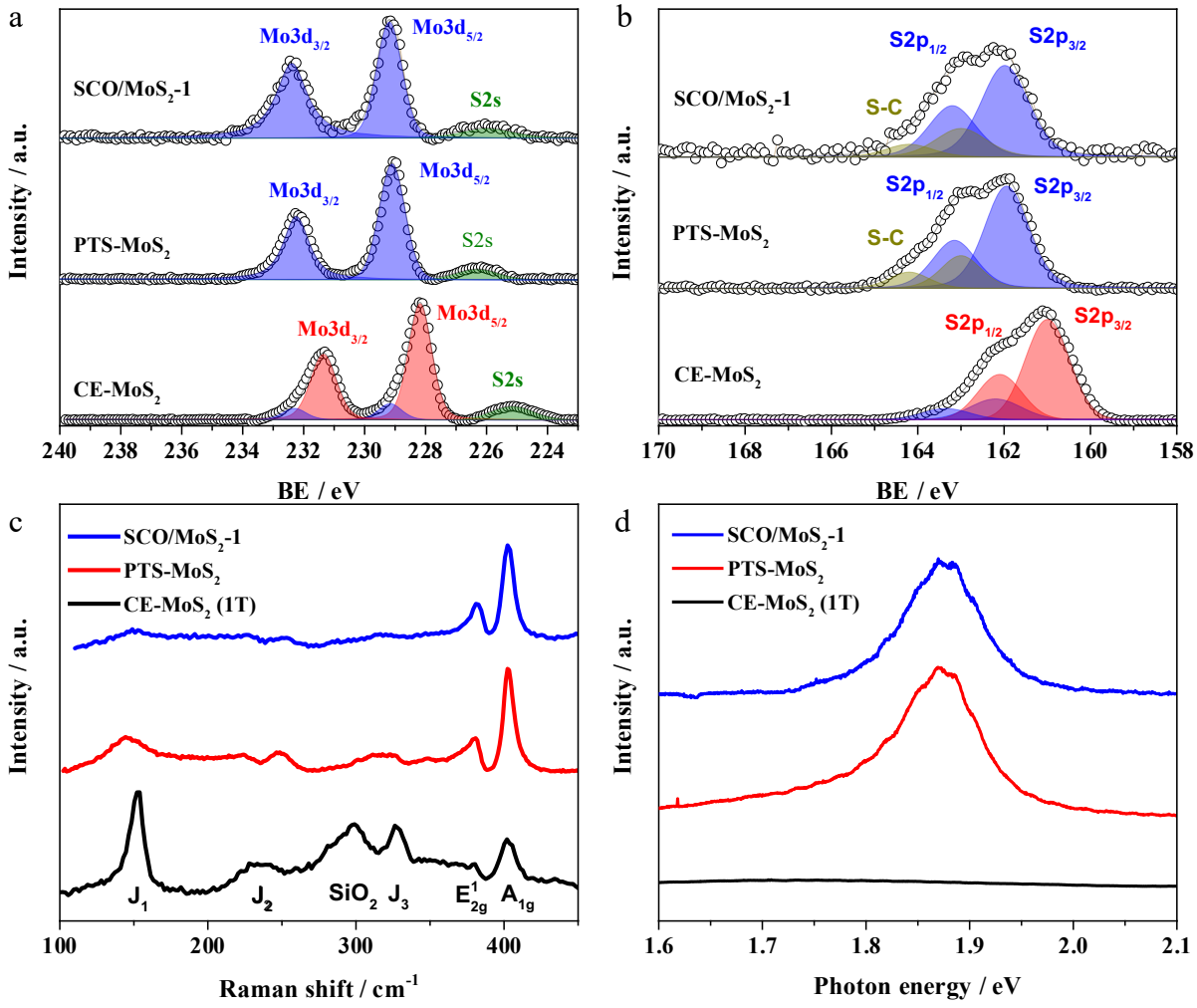

Fig. 2. CE-MoS_2, PTS-MoS_2, and SCO/MoS_2-1 spectroscopic characterization. a) Mo3d and b) S2p, deconvoluted high-resolution XPS spectra (blue, 2H-phase and red, 1T-phase contributions). c and d) Raman and PL spectra, respectively.

Spectroscopic studies are indicative of the formation of a covalent bond between the MoS_2 and the IPTS. C-S vibration is expected at ~690 cm^{-1} in the FTIR spectra. Although a signal is observed in this region, unfortunately, it overlaps with ethanol and IPTS vibrations, hindering a definitive assignation of this peak. Nevertheless, the appearance of an additional contribution at ~164 eV in the XPS S2p signal that modifies the deconvolution analysis, points out to functionalization of sulphur.[49] An additional support for this covalent functionalization comes

from energy-dispersive X-ray spectroscopy (EDAX) analysis performed on the thinnest flakes by a high resolution transmission electron microscope (HR-TEM). These results show the presence of silicon and the absence of iodine, while confirming that the integrity of the flakes is maintained after functionalization (**Fig. S3)**.

In order to anchor the SCO-NPs to the functionalized layers forming the final heterostructure (**SCO/MoS_2**), the methoxysilane groups decorating PTS-MoS_2 are used to graft the SCO-NPs silica shell by mixing both suspensions[41,45] (**Fig. 1**, step ii). In this way, we obtain MoS_2 functionalized with SCO-NPs bearing two aspect ratios (70 x 40 nm or 40 x 40 nm, **Fig. S4**,[44] SCO/MoS_2-**1** and SCO/MoS_2-**2a** respectively, **Fig. S5**) and three coverage degrees, accounted by the Fe:Mo ratios (See Methods, **Fig. S6**). The coexistence of the two components in the heterostructure is confirmed by HR-TEM (**Fig. 3a** and **S5-S6)** and XPS spectra, which exhibit the characteristic $Fe2p_{3/2}$ and $Fe2p_{1/2}$ peaks at ~709 eV and ~722 eV, respectively, coming from the SCO-NPs (**Fig. S7**) and similar Mo and S spectra to those recorded for PTS-MoS_2 (**Fig. 2a, b**). Finally, the integrity of the SCO-NPs in the hybrid is demonstrated by the magnetic data, which show a SCO thermal hysteresis very similar to the bulk, with transition temperatures at ~380 K ($T_{1/2}^{up}$) and ~340 K ($T_{1/2}^{down}$). **Fig. 3b and S8**.

Influence of the SCO-NPs on the properties of MoS_2 in the hybrid SCO/MoS_2 heterostructure. To study the potential of SCO-NPs to modify the electronic structure of MoS_2 layers, we rely on electrical transport and PL measurements. In most of the SCO/MoS_2 samples, we observe thermal hysteresis in the conductivities that follow well the SCO transitions observed from SQUID measurements.

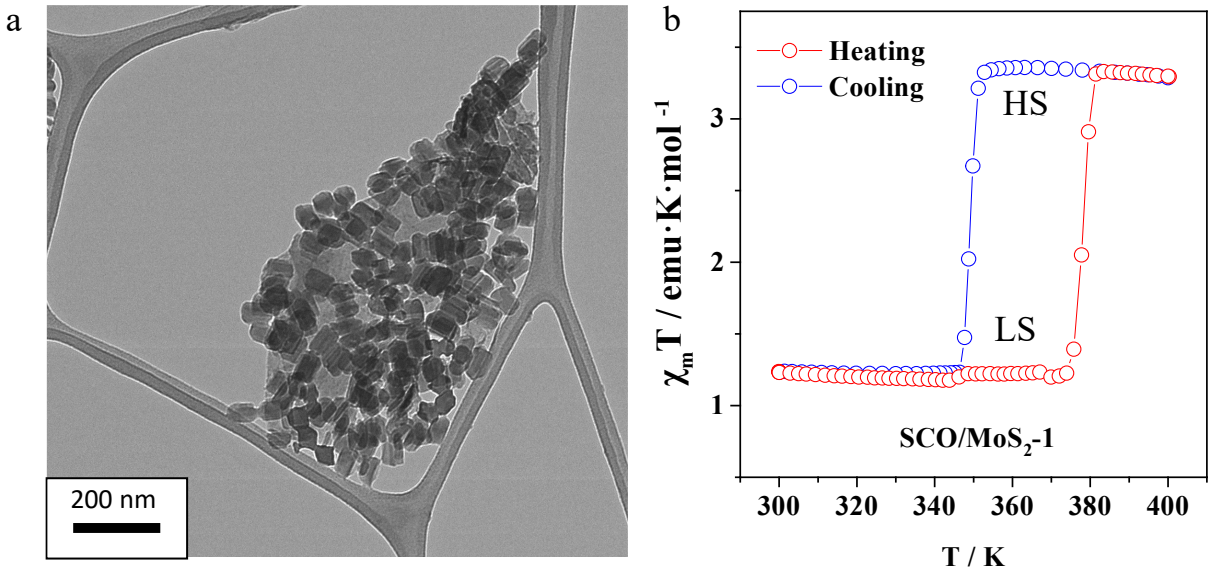

Fig. 3. Morphological and magnetic characterization of the SCO/MoS_2-1. a) HR-TEM image and b) thermal variation of the $\chi_M T$ product (being χ_M molar magnetic susceptibility) of the SCO/MoS_2-**1** (70 nm SCO-NPs on MoS_2 flakes with a Fe:Mo ratio of 2).

The strongest effects are obtained for heterostructures formed with SCO-NPs of 70 nm and a Fe:Mo ratio of 2, named SCO/MoS_2-**1**. As reported in **Fig. 4a**, this sample shows a sharp increase of ca.900% in the conductance upon heating, coincident with the spin transition from LS to HS ($T_{1/2}^{up} \approx 370$ K), and a sharp drop in conductance during the reversal cooling down process, corresponding to the transition from HS to LS ($T_{1/2}^{down} \approx 340$ K) (**Fig. 4a**). Remarkably, it presents an opposite behavior compared to the one observed for SCO-NPs (**Fig. 4b**), where the nanoparticles are less conductive in the LS state than in the HS. Keeping the Fe:Mo ratio equal to 2 but using smaller SCO-NPs of 40 nm (SCO/MoS_2-**2a**), the observed thermal variation in the electrical response is qualitatively similar, but with a smaller switch of ca.30% (**Fig. S9e-f**). This result points out that, when the relative quantity of SCO-compound: MoS_2 is maintained, there is a more relevant effect induced on the 2D material by the size and shape of the nanoparticles (whose axial elongation increases as their size does), than by their number.

Moreover, in SCO/MoS_2 hybrids the conductivity is up to 5 orders of magnitude larger than that of pure SCO-NPs (**Fig. S9**), overcoming the typical insulator character of the SCO compounds. This feature is also very important when dealing with the sample stability. In fact, a general problem encountered when measuring the transport in pure SCO-NPs is the high

voltages required (100 V), leading to a fast sample degradation.[52,53] On the contrary, the higher conductivities of the heteroestructures allow to measure at much lower voltages, thus guaranteeing sample integrity and the switching properties over several thermal cycles.

Additionally, we investigated the influence of the SCO-NPs/MoS_2 ratio on the transport properties, while keeping the shape and size of the particles unmodified. When the Fe:Mo ratio is further decreased from 2 to 0.4, SCO/MoS_2-**2b**, sample conductivity increases but the hysteretic effects coming from the SCO-NPs are completely lost, likely due to the low concentration of nanoparticles, **Fig. S9g**. Accordingly, sample conductivity decreases when the Fe:Mo ratio increases, and starting from a ratio of 5 (SCO/MoS_2-**2c)** sample behavior is reversed and approaches the one observed in assemblies of pure SCO-NPs, where the LS state becomes more conductive than the HS state[54,55] (**Fig. 4b and Fig. S9h**). From this reversal behavior in the conductivity of SCO/MoS_2 hybrids, we can conclude that for high concentrations of SCO-NPs, the charge transport is dominated by the nanoparticles. In contrast, when the concentration of the nanoparticles is decreased, the transport mainly occurs through the MoS_2 flakes.

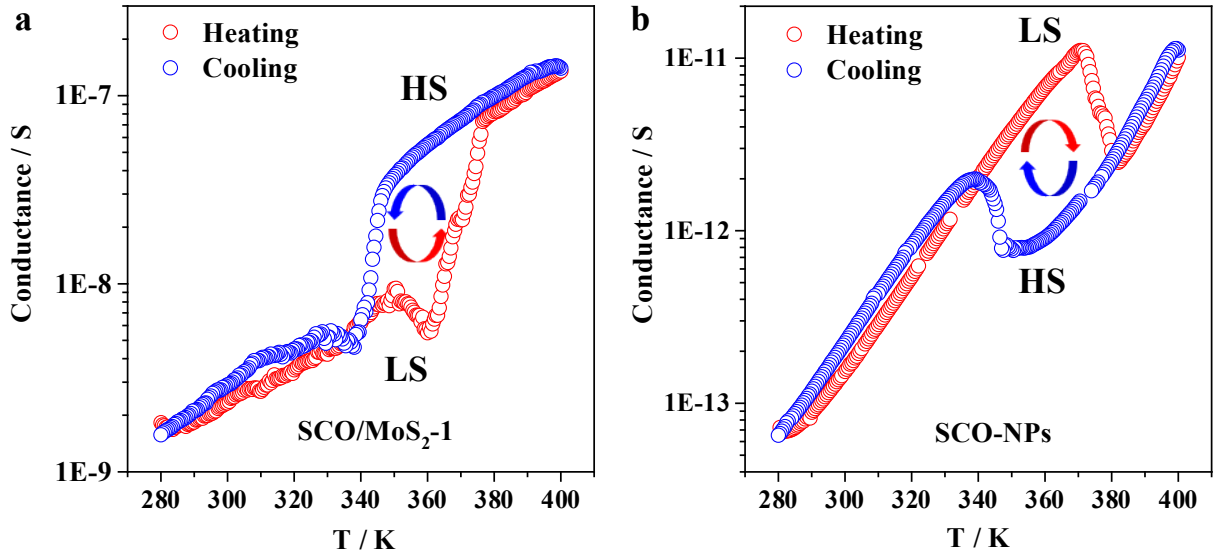

Fig. 4. Transport measurements. Thermal variation of the conductance in the heating and cooling modes for SCO/MoS_2-**1**, (a) and bare SCO-NPs, (b). The applied voltages were 2 V and 100 V, respectively. Thermal ramp was performed at 1 K·min^{-1},

These results suggest that the changes observed in the MoS_2 flakes come from the strain generated by the SCO-NPs. In this mechanism, the volume change of the nanoparticles induced by the spin transition is expected to strain the flakes, resulting in an intrinsic modulation of the band structure of the layers, and thus modifying their conductivity (for further details and discussion see Supplementary pages 11-16).[29]

Furthermore, because of the direct gap semiconductor nature of the MoS_2 monolayers (2H-phase), it is possible to gain direct information on their band gap energy through PL measurements.[51] In fact, it is well known that when a tensive strain is applied to a MoS_2 layer, its PL redshifts and weakens its intensity as consequence of a narrowing in the band gap and a transition in the semiconductor from direct to indirect band gap behavior occurs.[23,56] This is exactly the effect we have observed by Raman spectroscopy performed in the SCO/MoS_2-**1** hybrid in the two spin states (**Fig. 5a**). When the SCO-NPs are in the LS state (room temperature), a maximum in the PL signal (A peak) is observed at ~1.88 eV, which redshifts ~30-60 meV and decreases in intensity when the spin transition occurs (T > ~370). This variation can be monitored by measuring PL as a function of temperature, **Figure S12**. Complete cycles of heating and cooling are shown in **Fig. 5b**. We observe that the energy of the A peak presents a clear hysteretic behavior that completely resembles that of the spin state of the SCO-NPs. In the temperature range in which the spin state of the particles can be LS or HS, the A peak differs in intensity and energy at each temperature. This points out to a clear effect of the nanoparticles spin state on the MoS_2 band structure, additional to the thermal one.[57]

To further prove that this effect is induced by the SCO-NPs, we have performed a blank experiment on CE-MoS_2 transformed into the semiconducting 2H-phase by thermal treatment (**CE-MoS_2/2H**).[18] As can be observed in **Fig. S13**, the hysteretic behavior is absent in this case, being the A peak at each temperature completely independent of the heating or cooling path.

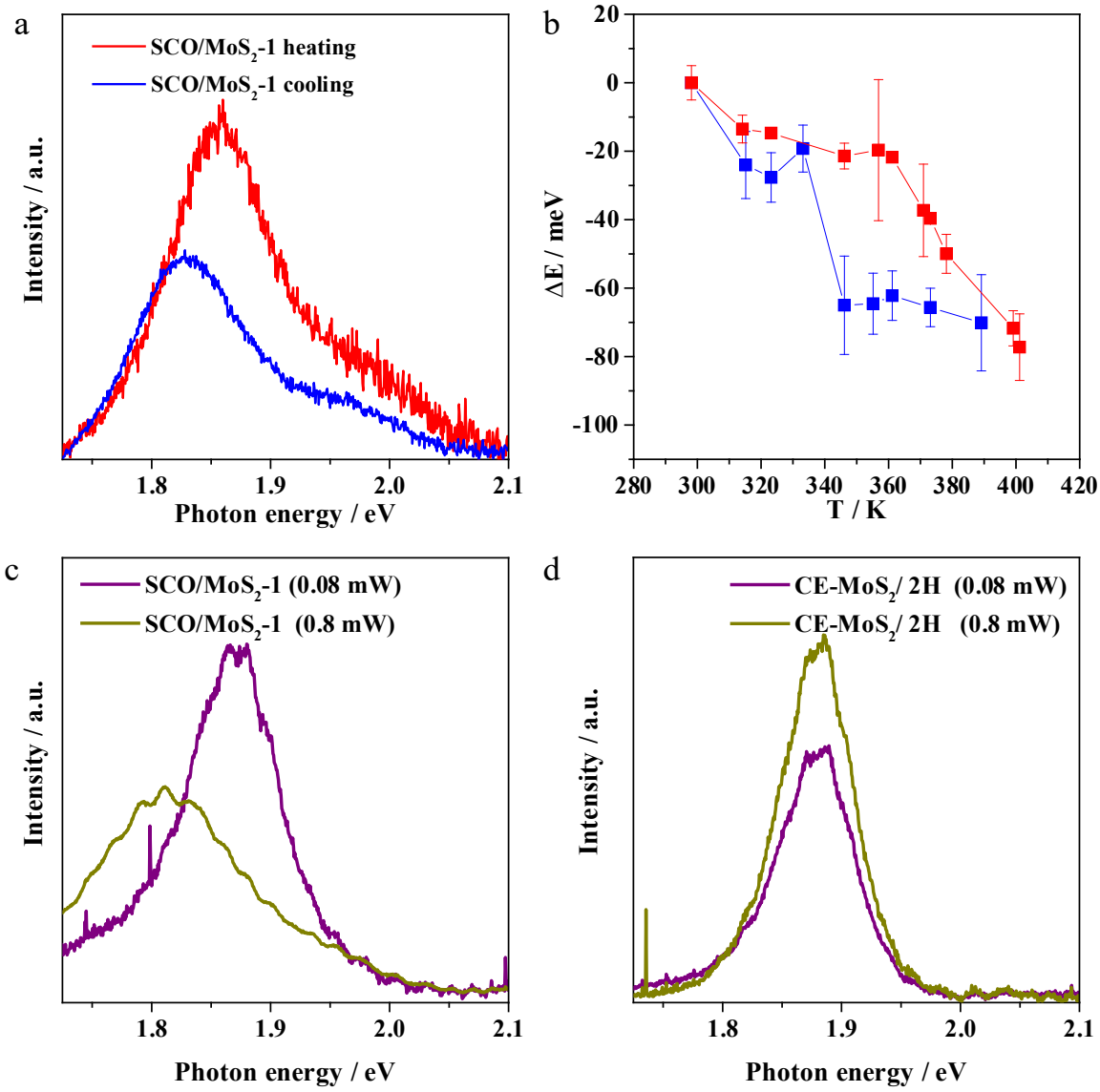

Fig. 5. Photoluminescence measurements. (a) PL spectra of SCO/MoS_2-**1** at LS, red line (heating), and HS states, blue line (cooling), taken at 355 K. (b) PL shift as a function of temperature (red dots, heating and blue dots, cooling). (c) and (d) PL spectra at two different laser intensities (0.8 mW, green and 0.08 mW, purple) of SCO/MoS_2-**1** and reference sample CE-MoS_2/2H, respectively (all the intensities have been normalized to the SiO_2 signal at 520 cm^{-1}).

Based on previous works,[56] the redshift observed in the SCO/MoS_2-**1** hybrid inside the temperature interval where the hysteresis loop is observed (i.e. ~ 40 meV at 355 K) corresponds to a ~0.6% of tensile strain, whereas the observed decrease of the PL intensity can be attributed to the increase in indirect band gap behaviour of the MoS_2 as a consequence of the strain.

Moreover, since the spin transition of the nanoparticles can be triggered by tuning the intensity of an irradiating light, the possibility of using an optical source to drive the PL of the

SCO/MoS_2-**1** hybrid was evaluated.[58] As shown in **Fig. 5c**, we measured the A peak of the hybrid at two green laser excitation intensities, 0.08 mW (purple curve), and 0.8 mW (green curve). For the lower intensity, the SCO-NPs in the heterostructure are in the LS state while for the higher one they are expected to undergo a spin transition to the HS state (**Fig. S14**). Under these conditions, SCO/MoS_2-**1** spectra show that the A peak redshifts of about 60 meV and decreases in intensity upon the laser power increase, as previously observed for thermal spin transition in **Fig. 5a.** Hence, these measurements prove that we can also optically induce a spin transition at room temperature by increasing the power of the excitation laser.

Comparing these results with the PL modulation thermally achieved, the shift of the A peak is clearly higher when a light source is used. This suggests a cooperative effect between the heating of the nanoparticles, due to laser irradiation, and the strain induced by the spin transition. Interestingly, when using CE-MoS_2/2H samples for blank measurements, we observe that under these laser intensities (0.8 and 0.08 mW), the PL remains unaffected (**Fig. 5d**), suggesting that MoS_2 is not directly heated by the laser in these experimental conditions, despite the fact that a thermal heating of the SCO-NPs is expected.[58] These studies thus demonstrate the possibility of inducing strain in the MoS_2 by light irradiation, opening the door to the fast optical modulation of 2D material properties. Moreover, as far as the spin state is concerned, it is possible to sense the spin in these SCO-NPs by following the change in the MoS_2 luminescence. This result is quite remarkable: on the one hand, because this kind of optical detection cannot be achieved in SCO/graphene heterostructures,[39] and, on the other, because we are providing a new tool for optical identification of spin states which is much more sensitive, simple and local than that obtained from transport measurements.

Discussion

We have reported here a two-step protocol in solution to chemically design smart molecular/2D heterostructures, formed by SCO-NPs covalently linked to semiconducting MoS_2 flakes. In a

first step, CE-MoS_2 flakes (metallic 1T-phase) have been covalently functionalized with an organic molecule (IPTS), which dramatically alters their electrical and optical properties and restores the semiconducting 2H-MoS_2 phase. Then, by means of the use of the attached molecules as grafting points, the SCO-NPs have been homogeneously anchored on these semiconducting MoS_2 layers, without further modification of the electronic structure of the 2D system. The robust synthetic methodology developed has permitted to obtain a family of SCO/MoS_2 covalently-linked heterostructures in which a control over the size of the nanoparticles and the degree of surface coverage has been achieved. This has led to a tunability in the resulting properties of the hybrids, which show a strong interplay between the spin transition and MoS_2 layers properties, leading to smart heterostructures that respond to external stimuli.

Regarding the 2D component, the change in volume of the SCO-NPs induced by the spin transition upon varying the temperature or by light irradiation, has generated a tensile strain on the MoS_2 layers which has been reflected by sharp changes in their electrical and optical properties. Notice that the present approach is radically different from those previously reported in this area,[25] in which the strain has been generated on pure MoS_2 layers by different strategies like the direct application of pressure on a suspended layer, with an AFM tip;[24] by using substrates that can transfer strain to the MoS_2 layer by a mechanical bending (in a flexible substrate)[23] or stretching (in an elastomeric substrate);[27] or by applying voltage (in a piezoelectric substrate),[59] or temperature (in a thermo-responsive substrate).[60] In contrast to all these cases, here the strain is generated in a single material, based on a chemically-designed hybrid heterostructure, either by a temperature modulation or by light irradiation. Hence, the intrinsic properties of the SCO component have opened the possibility for the first time, of using light as external stimulus to induce strain in TMDCs layers.

In conclusion, these innovative results demonstrate the fabrication of a multifunctional material where properties of the two components have been reciprocally boosted. Compared to pure

SCO-NPs, MoS_2 confers to this hybrid luminescence and higher resilience and conductance. Concurrently, MoS_2 gains new degrees of freedom thanks to SCO-NPs spin which can be addressed by temperature or light and read-out electrically or optically.

All in all, a new smart heterostructure which mimics the bistability displayed by spin-crossover materials but ignores the typical drawbacks of these compounds have been synthesized. Interestingly, our approach could be easily expanded to other 2D materials offering a yet unexplored modulation of their properties and opening new frontiers for strain engineering, towards their application in multifunctional devices for beyond conventional electronics.

Methods

Materials. All chemical reagents were purchased and used without further purification: (3-Iodopropyl)trimethoxysilane, 1-Iodooctadecane (Sigma-Aldrich), Tetraethyl orthosilicate 98% (Sigma-Aldrich), Triton X-100 (Sigma-Aldrich), ascorbic acid (Sigma-Aldrich), 1,2,4-triazole (Sigma-Aldrich), iron tetrafluoroborate hexahydrate (Sigma-Aldrich), n-hexanol (Sigma-Aldrich), cyclohexane (Sigma-Aldrich, ethanol absolute (Sigma-Aldrich) ultra-pure water (18.2 MΩ). Molybdenum(IV) sulfide (Alfa Aesar), *n*-butyllithium solution 1.6 M in hexane (Sigma-Aldrich), anhydrous hexane (Sigma-Aldrich). SiO_2 (285 nm)/Si substrates were bought from NOVA Electronic Materials LLC, Flower Mound, TX.

Chemical exfoliation MoS_2 (CE-MoS_2). The chemical exfoliation of MoS_2 was carried out according to the experimental protocol reported by M. Morant-Giner et al.[48]

Chemical exfoliated MoS_2 in 2H-phase.

CE-MoS_2 flakes retrieved by centrifugation is spin coated on SiO_2 (285 nm)/Si substrates and heated up at 200ºC for 2 h under an inert atmosphere (O_2 < 0.1 ppm, H_2O < 0.1 ppm), to induce the 1T-to-2H-phase transition

70 x 50 nm [Fe(Htrz)(trz)(BF_4)]@SiO_2 Nanoparticles. The nanoparticles were synthetized following a strategy very close to that previously reported in by R. Torres-Cavanillas et al.[44] but with slight modifications. An aqueous solution of $Fe(BF_4)_2 \cdot 6H_2O$ (0.5 mL, 1.25 M) and

tetraethyl orthosilicate (TEOS) (0.1 mL) is added to a freshly prepared mixture containing Triton X-100 (1.8 mL, ω = 9), n-hexanol (1.8 mL), cyclohexane (7.5 mL). A microemulsion of this mixture is obtained by stirring at room temperature during 15 minutes. Then, an aqueous solution of 1,2,4-1H-triazole (0.5 mL, 4.5 M) ligand containing the TEOS (0.1 mL) is added to a similarly prepared organic solution and stirred at room temperature for 15 min. In order to permit a micellar exchange, both microemulsions are combined and stirred for 2 h. The formed nanoparticles are isolated by precipitation upon addition of acetone and collected by centrifugation (12000 rpm, 10 min), followed by washing with ethanol (x4 times), to remove the excess of surfactant, and acetone (x1 time). Finally, the powdered samples are dried at 70ºC for 2 h.

40 x 40 nm [Fe(Htrz)(trz)(BF_4)]@SiO_2 NPs. The synthesis of the smallest NPs follows the same procedure as for the 70 nm but using 2 mL of Triton X.100.

MoS_2 IPTS functionalization (PTS-MoS_2). Firstly, a 5 mM aqueous suspension of CE-MoS_2 flakes is prepared from the mother one. Independently, a solution of 3-iodopropyl(trimethoxysilane) (IPTS), 0.1 M in ethanol is prepared. Later the IPTS solution is slowly added over the aqueous suspension in water:ethanol ratio, 2:1, under strong stirring, and let it react for 12h. Finally, the functionalized nanosheets are washed by several cycles of centrifugation (at 7000 rpm, 15 min) and dispersed in water:ethanol, 2:1 (x3 times), and in ethanol (x3 times).

SCO/MoS_2. The functionalized PTS-MoS_2 is suspended in ethanol under vigorous stirring in a concentration of 5 mM. Later, a colloidal suspension of 70 nm SCO-NPs, 10 $mg \cdot ml^{-1}$, is added and leave it to react for 48 h. Finally, several cycles of centrifugation and dispersion at different rates are carried out until the supernatant has no residues of SCO-NPs. Induced coupled plasma optical emission spectrometry (ICP-OES) of acid-digested samples, indicates a Fe:Mo ratio of 2:1. (SCO/MoS_2-**1**).

For the synthesis of the analogue hybrid with smaller size nanoparticles, at different Fe:Mo ratios, an equivalent procedure was followed but adding 40 nm SCO-NPs suspension in 10, 1, or 20 $mg \cdot ml^{-1}$ for: SCO/MoS_2-**2a**, SCO/MoS_2-**2b** and SCO/MoS_2-**2c,** respectively. ICP-OES Fe:Mo ratios of 2:1 for SCO/MoS_2-**2a**, 0.4:1 for SCO/MoS_2-**2b** and 5:1 for SCO/MoS_2-**2c** are measured.

Author Contributions

R.T-C. and M.M-G. contributed equally to this work. R. T.-C. was responsible of the design, synthesis and characterization of the new heterostructure and was involved in all the experimental measurements, discussion and preparation of the manuscript. M. M-G was in charge of the preparation of the exfoliated material and help with all characterization steps of the new system. M. G. was in charge of all transport characterization where, G. E-A, J. D. and S. T. were involved. S. C.-S. helped with discussion and theoretical interpretation of the observed properties. M. G.-M. contributed to the SCO-NPs preparation and the discussion and interpretation of results. J. C.-F. was involved in all photoluminescence experiments and interpretation. A. F.-A. designed the work and was involved in the development and coordination of all experimental parts, discussion of results and preparation of the manuscript. E. C. supervised all the work and the preparation of the manuscript. All authors revised and contributed to the presented manuscript.

Supplementary Information

Supplementary Information is available.

Acknowledgments

The authors acknowledge the financial support from the EU (ERC-Advanced Grant MOL-2D, FET-OPEN COSMICS 766726 and COST-MOLSPIN CA15128), the Spanish MINECO (Grants MAT2017-89993, Excellence Unit María de Maeztu MDM-2015-0538, RTI2018-098568-A-I and EQC2018-004888-P, cofinanced by FEDER), and the Generalitat Valenciana

(Prometeo Program of Excellence, PO FEDER Program, ref. IDIFEDER/2018/061, and GentT Program, ref. CIDEGENT/2018/005). Spanish MINECO is also acknowledged for two predoctoral fellowships (to R.T.-C. and M.M.-G), two Juan de la Cierva Incorporación postdoctoral Grants (to S.C.-S. and M.G.) and a Ramón y Cajal Contract (RYC-2016-19817) (to S.T.). M.G.-M thanks support from "la Caixa" Foundation (LCF/BQ/PI19/11690022) and Generalitat Valenciana (SEJI/2020/036). A.F.-A. thanks the Universitat de València for a Senior Researcher contract. The authors are very grateful to Prof. J. M. Herrera from the Dept. of Inorganic Chemistry (Universidad de Granada) for his helpful discussion about core-shell spin-crossover nanoparticles.

1. Stanford, M. G., Rack, P. D. & Jariwala, D. Emerging nanofabrication and quantum confinement techniques for 2D materials beyond graphene. *npj 2D Materials and Applications* **2,** 768–15 (2018).
2. Wang, L. *et al.* One-Dimensional Electrical Contact to a Two-Dimensional Material. *Science* **342,** 614–617 (2013).
3. Xia, W. *et al.* Recent progress in van der Waals heterojunctions. *Nanoscale* **9,** 4324–4365 (2017).
4. Onga, M. *et al.* Antiferromagnet-Semiconductor Van Der Waals Heterostructures: Interlayer Interplay of Exciton with Magnetic Ordering. *Nano Lett.* **20,** 4625–4630 (2020).
5. Hirsch, A. & Hauke, F. Post-Graphene 2D Chemistry: The Emerging Field of Molybdenum Disulfide and Black Phosphorus Functionalization. *Angew. Chem. Int. Ed.* **57,** 4338–4354 (2018).
6. López-Cabrelles, J. *et al.* Isoreticular two-dimensional magnetic coordination polymers prepared through pre-synthetic ligand functionalization. *Nature Chemistry* **10,** 1001–1007 (2018).
7. Rodríguez-San-Miguel, D., Montoro, C. & Zamora, F. Covalent organic framework nanosheets: Preparation, properties and applications. *Chem. Soc. Rev.* **49,** 2291–2302 (2020).
8. Jariwala, D., Marks, T. J. & Hersam, M. C. Mixed-dimensional van der Waals heterostructures. *Nat Mater* **16,** 170–181 (2017).
9. Choi, J., Zhang, H. & Choi, J. H. Modulating Optoelectronic Properties of Two-Dimensional Transition Metal Dichalcogenide Semiconductors by Photoinduced Charge Transfer. *ACS Nano* **10,** 1671–1680 (2016).
10. Das, S., Robinson, J. A., Dubey, M., Terrones, H. & Terrones, M. in *Annual Review of Materials Research* **45,** 1–27 (2015).
11. Manzeli, S., Ovchinnikov, D., Pasquier, D., Yazyev, O. V. & Kis, A. 2D transition metal dichalcogenides. *Nat. Rev. Mater.* **2,** (2017).
12. Hu, Z. *et al.* Two-dimensional transition metal dichalcogenides: Interface and defect engineering. *Chem. Soc. Rev.* **47,** 3100–3128 (2018).
13. Ganatra, R. & Zhang, Q. Few-layer MoS_2: A promising layered semiconductor. *ACS Nano* **8,** 4074–4099 (2014).

14. Kan, M. *et al.* Structures and phase transition of a MoS_2 monolayer. *J. Phys. Chem. C* **118,** 1515–1522 (2014).
15. Wang, L., Xu, Z., Wang, W. & Bai, X. Atomic mechanism of dynamic electrochemical lithiation processes of MoS_2 nanosheets. *J. Am. Chem. Soc.* **136,** 6693–6697 (2014).
16. Yuwen, L. *et al.* Rapid preparation of single-layer transition metal dichalcogenide nanosheets via ultrasonication enhanced lithium intercalation. *Chem. Commun.* **52,** 529–532 (2015).
17. Lin, Y.-C., Dumcenco, D. O., Huang, Y.-S. & Suenaga, K. Atomic mechanism of the semiconducting-to-metallic phase transition in single-layered MoS_2. *Nature Nanotech* **9,** 391–396 (2014).
18. Eda, G. *et al.* Photoluminescence from chemically exfoliated MoS_2. *Nano Lett.* **11,** 5111–5116 (2011).
19. Fan, X. *et al.* Fast and Efficient Preparation of Exfoliated 2H MoS_2 Nanosheets by Sonication-Assisted Lithium Intercalation and Infrared Laser-Induced 1T to 2H Phase Reversion. *Nano Lett.* **15,** 5956–5960 (2015).
20. Yang, D., Sandoval, S. J., Divigalpitiya, W. M. R., Irwin, J. C. & Frindt, R. F. Structure of single-molecular-layer MoS_2. *Phys. Rev. B* **43,** 12053–12056 (1991).
21. Yun, W. S., Han, S. W., Hong, S. C., Kim, I. G. & Lee, J. D. Thickness and strain effects on electronic structures of transition metal dichalcogenides: 2H-MX_2 semiconductors (M = Mo, W; X = S, Se, Te). *Phys. Rev. B Condens. Matter Mater. Phys.* **85,** 033305 (2012).
22. Ouyang, B., Xiong, S., Yang, Z., Jing, Y. & Wang, Y. MoS_2 heterostructure with tunable phase stability: Strain induced interlayer covalent bond formation. *Nanoscale* **9,** 8126–8132 (2017).
23. Conley, H. J. *et al.* Bandgap Engineering of Strained Monolayer and Bilayer MoS 2. *Nano Lett.* **13,** 3626–3630 (2013).
24. Manzeli, S., Allain, A., Ghadimi, A. & Kis, A. Piezoresistivity and Strain-induced Band Gap Tuning in Atomically Thin MoS_2. *Nano Lett.* **15,** 5330–5335 (2015).
25. Sun, Y. & Liu, K. Strain engineering in functional 2-dimensional materials. *J Appl Phys* **125,** 082402–12 (2019).
26. Yang, R. *et al.* Tuning Optical Signatures of Single- and Few-Layer MoS 2by Blown-Bubble Bulge Straining up to Fracture. *Nano Lett.* **17,** 4568–4575 (2017).
27. Castellanos-Gomez, A. *et al.* Local strain engineering in atomically thin MoS_2. *Nano Lett.* **13,** 5361–5366 (2013).
28. Tsai, M.-Y. *et al.* Flexible MoS_2 Field-Effect Transistors for Gate-Tunable Piezoresistive Strain Sensors. *ACS Appl. Mater. Interfaces* **7,** 12850–12855 (2015).
29. Biccai, S. *et al.* Negative Gauge Factor Piezoresistive Composites Based on Polymers Filled with MoS_2 Nanosheets. *ACS Nano* **13,** 6845–6855 (2019).
30. Grosjean, A. *et al.* Crystal structures and spin crossover in the polymeric material $[Fe(Htrz)_2(trz)](BF_4)$ including coherent-domain size reduction effects. *Eur. J. Inorg. Chem.* 796–802 (2013).
31. Dugay, J. *et al.* Sensing of the Molecular Spin in Spin-Crossover Nanoparticles with Micromechanical Resonators. *J. Phys. Chem. C* **123,** 6778–6786 (2019).
32. Coronado, E., Galán-Mascarós, J. R., Monrabal-Capilla, M., García-Martínez, J. & Pardo-Ibáñez, P. Bistable Spin-Crossover Nanoparticles Showing Magnetic Thermal Hysteresis near Room Temperature. *Adv Mater* **19,** 1359–1361 (2007).
33. Rotaru, A. *et al.* Spin state dependence of electrical conductivity of spin crossover materials. *Chem. Commun.* **48,** 4163–4165 (2012).
34. Boldog, I. *et al.* Spin-crossover nanocrystals with magnetic, optical, and structural bistability near room temperature. *Angew. Chem. Int. Ed.* **47,** 6433–6437 (2008).

35. Shepherd, H. J. *et al.* Molecular actuators driven by cooperative spin-state switching. *Nat. Commun.* **4,** 1–9 (2013).
36. Koo, Y.-S. & Galán-Mascarós, J. R. Spin Crossover Probes Confer Multistability to Organic Conducting Polymers. *Adv Mater* **26,** 6785–6789 (2014).
37. Chen, Y.-C., Meng, Y., Ni, Z.-P. & Tong, M.-L. Synergistic electrical bistability in a conductive spin crossover heterostructure. *J. Mater. Chem. C* **3,** 945–949 (2015).
38. Rat, S. *et al.* Coupling Mechanical and Electrical Properties in Spin Crossover Polymer Composites. *Adv Mater* **30,** 1705275–6 (2018).
39. Dugay, J. *et al.* Phase Transitions in Spin-Crossover Thin Films Probed by Graphene Transport Measurements. *Nano Lett.* **17,** 186–193 (2017).
40. Geest, E. P. *et al.* Contactless Spin Switch Sensing by Chemo-Electric Gating of Graphene. *Adv. Mater. (Weinheim, Ger.)* **32,** 1903575–9 (2020).
41. Titos-Padilla, S., Herrera, J. M., Chen, X.-W., Delgado, J. J. & Colacio, E. Bifunctional hybrid SiO_2 nanoparticles showing synergy between core spin crossover and shell luminescence properties. *Angew. Chem. Int. Ed.* **50,** 3290–3293 (2011).
42. Herrera, J. M. *et al.* Studies on bifunctional Fe(II)-triazole spin crossover nanoparticles: Time-dependent luminescence, surface grafting and the effect of a silica shell and hydrostatic pressure on the magnetic properties. *J. Mater. Chem. C* **3,** 7819–7829 (2015).
43. Giménez-Marqués, M., García-Sanz de Larrea, M. L. & Coronado, E. Unravelling the chemical design of spin-crossover nanoparticles based on iron(II)-triazole coordination polymers: Towards a control of the spin transition. *J. Mater. Chem. C* **3,** 7946–7953 (2015).
44. Torres-Cavanillas, R. *et al.* Downsizing of robust Fe-triazole@SiO_2 spin-crossover nanoparticles with ultrathin shells. *Dalton Trans.* **1,** 1–5 (2019).
45. Ulman, A. Formation and Structure of Self-Assembled Monolayers. *Chem. Rev.* **96,** 1533–1554 (1996).
46. Joensen, P., Frindt, R. F. & Morrison, S. R. Single-layer MoS_2. *Mat. Res. Bull.* **21,** 457–461 (1986).
47. Leng, K. *et al.* Phase Restructuring in Transition Metal Dichalcogenides for Highly Stable Energy Storage. *ACS Nano* **10,** 9208–9215 (2016).
48. Morant-Giner, M. *et al.* Prussian Blue@MoS_2Layer Composites as Highly Efficient Cathodes for Sodium- and Potassium-Ion Batteries. *Adv. Funct. Mater.* **28,** 1706125 (2017).
49. Voiry, D. *et al.* Covalent functionalization of monolayered transition metal dichalcogenides by phase engineering. *Nature Chemistry* **7,** 45–49 (2015).
50. Saito, R., Tatsumi, Y., Huang, S., Ling, X. & Dresselhaus, M. S. Raman spectroscopy of transition metal dichalcogenides. *J Phys Condens Matter* **28,** (2016).
51. Splendiani, A. *et al.* Emerging Photoluminescence in Monolayer MoS_2. *Nano Lett.* **10,** 1271–1275 (2010).
52. Rotaru, A. *et al.* Nano-electromanipulation of spin crossover nanorods: Towards switchable nanoelectronic devices. *Adv Mater* **25,** 1745–1749 (2013).
53. Molnár, G., Rat, S., Salmon, L., Nicolazzi, W. & Bousseksou, A. Spin Crossover Nanomaterials: From Fundamental Concepts to Devices. *Adv Mater* **30,** (2018).
54. Dugay, J. *et al.* Spin switching in electronic devices based on 2D assemblies of spin-crossover nanoparticles. *Adv Mater* **27,** 1288–1293 (2015).
55. Dugay, J. *et al.* Charge Mobility and Dynamics in Spin-Crossover Nanoparticles Studied by Time-Resolved Microwave Conductivity. *Journal of Physical Chemistry Letters* **9,** 5672–5678 (2018).

56. Pető, J. *et al.* Moderate strain induced indirect bandgap and conduction electrons in MoS_2 single layers. *npj 2D Materials and Applications* **3,** 5836–6 (2019).
57. Korn, T., Heydrich, S., Hirmer, M., Schmutzler, J. & Schller, C. Low-temperature photocarrier dynamics in monolayer MoS_2. *Appl Phys Lett* **99,** (2011).
58. Guillaume, F. *et al.* Photoswitching of the spin crossover polymeric material [Fe(Htrz) $_2$ (trz)](BF $_4$) under continuous laser irradiation in a Raman scattering experiment. *Chemical Physics Letters* **604,** 105–109 (2014).
59. Hui, Y. Y. *et al.* Exceptional tunability of band energy in a compressively strained trilayer MoS_2 sheet. *ACS Nano* **7,** 7126–7131 (2013).
60. Gant, P. *et al.* A strain tunable single-layer MoS_2 photodetector. *Materials Today* **27,** 8–13 (2019).